Macromolecules

pubs.acs.org/Macromolecules Article

Chain Dimension and Dynamics of Polymers in Well-Defined Non-sticky Nanocomposites of Molecular Nanoparticle Polyhedral Oligomeric Silsesquioxane/Poly(butylene oxide)

Xinlin Zhang, Wei Wei, Xin Jin, and Huiming Xiong*

Cite This: https://dx.doi.org/10.1021/acs.macromol.0c00158 Read Online

ACCESS | Metrics & More | Article Recommendations | Supporting Information

ABSTRACT: The chain dimension and dynamics of type-A polymer, poly(1, 2-butylene oxide) (PBO), in the nanocomposites comprising polyhedral oligomeric silsesquioxane (POSS) nanoparticles have been investigated in broad frequency and temperature windows by utilizing broadband dielectric spectroscopy and rheology. Non-crystalline and dielectric "invisible" molecular nanoparticle POSS was specially designed to ensure its miscibility with the PBO matrix, which was verified by quantitative estimation of solubility parameters and subsequent X-ray scattering experiments. Dispersions of POSS in the PBO matrix up to 10 vol % have been investigated. Dielectric experiments revealed a negligible change of the dielectric relaxation strength of the normal mode and thus the statistical chain dimension of PBO, regardless of the POSS loadings and the polymer chain lengths spanning from the unentangled to the entangled region. The introduction of nanoparticles is found to influence both the chain and segment dynamics when the molecular weight of the polymer is relatively low. However, by renormalized with the segmental relaxation, the dielectric chain relaxation shows identical characteristic relaxation time with that of the neat polymer, independent of the volume fractions of POSS, which is consistent with the terminal relaxation time determined in the rheology experiments. The slowing down of segmental relaxation has been attributed to the influence of nanoparticles on the chain ends associated with excess free volume. The possible confinement, solvent, and filler effects in this type of a non-sticky nanocomposite model system have been further discussed.

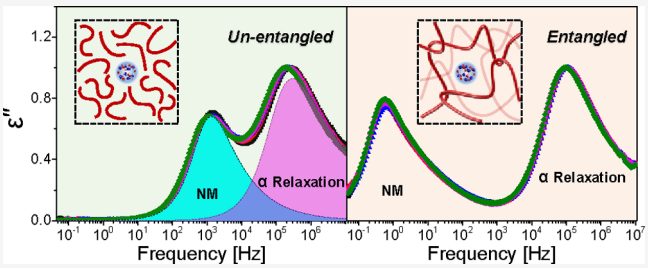

1. INTRODUCTION

Polymer nanocomposites (PNCs) have attracted tremendous interests both in the academic and industrial fields.[1−11] In general, the enhanced performance and properties of the PNCs depend on the nature of the nanoparticles, such as their size, shape, softness, and surface, the sign and strength of the interaction between the nanoparticles and polymer matrix, the dispersion state of the nanoparticles, and so on. Despite the extensive research on PNCs, fundamental understanding of the effects of the nanoparticles on chain conformation and dynamics of the host polymer remains to be explored and scientifically interesting.[12−19]

In non-sticky systems, the relative size of nanoparticles and polymers has been proposed to be a key parameter to control the miscibility and chain dimension, which has been investigated in extensive experiments and simulations. When cross-linked polystyrene (PS) nanoparticles were dispersed in the chemically identical PS matrix at 10 vol %, it was found that they were immiscible if the radius of gyration (Rg) of the PS matrix was smaller than the radius of nanoparticles (R_N), while the chain was swollen by 20% if Rg ≥ R_N.[5,13,20] For the trimethylsilyl-treated polysilicate particles/PDMS system, chain expansion greater than 60% was found when Rg > R_N, while contraction occurred when Rg ≈ R_N.[21] No measurable change was observed in the miscible phenyl coating silica/PS nanocomposite system up to 32.7 vol % at Rg/R_N ≈ 1.9−3.9 by utilizing small-angle neutron scattering (SANS).[15] In the hydrophobic silica/PEP nanocomposite, reduction of the chain dimension at Rg/R_N ≈ 0.5 and no change at Rg/R_N ≈ 2 were observed.[16] Both experiments and simulations on the weakly interacting system of pentyl-coated SiO_2/PS (R_N/Rg = 1−8, R_N = 3−6.5 nm) showed identical chain dimension with the neat polymer independent of the nanoparticle volume fraction and the length of the host polymer,[14,17,22,23] while a decrease in the chain dimension with an increase in the nanoparticle loading at Rg/R_N ≈ 1.2 was demonstrated in the simulation.[24]

The sign of interaction is also a critical factor to influence the chain conformation in PNCs. When the interaction between the nanoparticle and the polymer matrix was attractive, no significant change of the chain dimension in the silica/poly(methyl methacrylate) (PMMA) nanocomposite

Received: January 21, 2020
Revised: May 4, 2020

ACS Publications © XXXX American Chemical Society

was observed in SANS at silica loading up to 30 vol % despite forming aggregates.[23] Different polymer−particle interactions from attractive to repulsive were achieved in the Fe_2O_3/PS nanocomposite by grafting the PS chains. The SANS extrapolation method elucidated swelling of the chain for the bare nanoparticle, while polymer chains were either unchanged or compressed for the grafted nanoparticle depending on the dispersion state.[18] The simulation demonstrated chain contraction in weakly attractive and repulsive interactions with nanoparticle loading up to 51 vol % at $Rg/R_N \approx 1.2$,[24] while chain stretching and expanding at high nanoparticle loading were also reported.[19] In attractive systems, a bound layer or interphase layer surrounding the nanoparticle is usually present, which can also influence the properties of PNCs, chain conformations, and dynamics dramatically.[25−27]

The presence of nanoparticles in PNCs could affect the hierarchical dynamics of the host polymers in a comprehensive way, and the probed dynamics rely exclusively on the employed characterization techniques.[12,28−33] In the non-attractive silica/PEP system, the transition from the topologic entanglement to the geometric entanglement imposed by nanoparticles was elucidated by means of neutron spin echo spectroscopy and rheology experiments, wherein the basic Rouse relaxation was found unaffected even at high nanoparticle contents.[30,31] In the phenyl-capped silica/PS nanocomposite, the center of mass diffusion of polymers probed by an elastic recoil detection method was found to be slowed down due to the entropy loss of chain conformation.[32,34,35] A recent study on the attractive silica/P2VP system by rheology and dielectric measurements revealed unchanged chain relaxation and slowed segmental dynamics.[36] In the tetrasulfidosilane-coated silica/poly(vinyl acetate) system, the segmental relaxation remained the same with the nanoparticle content up to 28 vol %,[37] while enhanced segmental dynamics was observed in the POSS/PS nanocomposite.[38]

The sophisticated effects of nanoparticles on chain conformation and dynamics can be ascribed to the intrinsic complexity of the composite system, including the diverse features of nanoparticles, the existence of the interface or interphase, and various nanoparticle−polymer interactions on the one hand; on the other hand, the hierarchical structures and dynamics of polymers on multiple length scales and time scales impart additional complexities. Practically, good dispersion under structural control could be an appropriate starting point to achieve a comprehensive understanding. Meanwhile, a combination of diverse methods in distinct time−space is highly desirable, although it is often challenging and limited in reality.

Broadband dielectric spectroscopy (BDS) is a powerful technique in studying molecular dynamics associated with fluctuation of dipole moment, which is capable to access a very broad dynamic window.[39] Particularly, for type-A polymers in the Stockmayer classification,[40,41] the dipole moments fixed along the backbone do not cancel at the whole chain, which can generate an end-to-end net polarization vector. Fluctuation of this type of end-to-end vector reflects the so-called normal mode (NM) relaxation, which strength is associated with the mean-square end-to-end distance of the chain and the peak position is characteristic of the global chain dynamics.[39−46] Moreover, relaxation of perpendicular dipolar components generally present in the polymers can be also probed, which are usually associated with segmental relaxation and other local modes.[39] As such, BDS is superior in simultaneous exploration of hierarchical relaxation processes and their correlation in a quantitative way.

Poly(1,2-butylene oxide) (PBO) is such a typical type-A polymer,[29,47−51] which can be synthesized through anionic ring-opening polymerization. Well-defined polymers with controlled molecular weight, discrete end groups, and narrow dispersity can thus be obtained as demonstrated in this work. Besides, the relatively low glass transition temperature of PBO can facilitate the composite system to reach the equilibrium state readily and the processing at a high temperature can be avoided. To construct our PNC system, the so-called molecular nanoparticle, polyhedral oligomeric silsesquioxane (POSS), with well-defined shape and size (core diameter around 1 nm) is chosen, which is regarded as the smallest silica particle. More importantly, POSS can be subjected to precise chemical modification to achieve desired properties, for example, to obtain a non-crystalline motif possessing identical cohesive energy with that of PBO. Consequently, a good dispersion between POSS and PBO can thus be achieved. In dielectrics, PBO has a comparably high strength of dielectric normal mode relaxation, while the rigid and symmetric POSS does not relax within the interested frequency window. This remarkable dielectric "invisibility" of POSS allows to exclusively probe the conformation and dynamics of polymers in the composite system. The molecular weight of PBO in our work spans from the unentangled to the entangled regime. By combining BDS and rheology experiments, our nanocomposite system has been served as a model system to address the effects of nanoparticles on the chain dimension and dynamics of polymers in the PNCs as a function of POSS content. The possible solvent, confinement, and filler effects in this athermal system are also discussed.

2. EXPERIMENTAL SECTION

2.1. Materials. 1,2-Butylene oxide (BO) was dried over CaH_2 and then distilled into a vacuumed flask containing dibutylmagnesium to remove traces of impurities. 18-Crown-6 (99%, Sigma-Aldrich), 2-methyl-3-buten-2-ol (98+%, Adamas), trichloropropylsilane (99%, TCI), and trisilanolisooctyl POSS (99%, Hybrid Plastics) were used as received. All other reagents were analytical grade and used as received. All solvents were purified by distillation.

2.2. Characterization Methods. The nuclear magnetic resonance spectroscopy (NMR) spectra were recorded on a Bruker-500 (500 MHz, ^{1}H NMR) spectrometer with chemical shifts reported in ppm relative to the residual deuterated $CDCl_3$ solvent. Gel permeation chromatography (GPC) with a multiangle laser light scattering detector (Wyatt Dawn EOS) plus a differential refractometer detector (Waters Model 2414) was used to determine the weight-averaged molecular weight (M_w), number-averaged molecular weight (M_n), and polymer dispersity index (PDI; M_w/M_n). The matrix-assisted laser desorption/ionization time-of-flight mass spectrometry (MALDI-TOF MS) spectra were recorded on Autoflex Speed MALDI TOF/TOF (Bruker Dalonics, Inc., Billarica, MA), equipped with a Nd:YAG laser emitting at a wavelength of 355 nm. The instrument was calibrated externally with a PMMA standard prior to each measurement. *trans*-2-[3-(4-*tert*-Butylphenyl)-2-methylpropenylidene]malononitrile (DCTB) and sodium trifluoroacetate (NaTFA) served as the matrix and cationization salt, respectively.

Wide-angle X-ray diffraction (WAXD) measurements were carried out on the synchrotron X-ray beamline BL16B in the Shanghai Synchrotron Radiation Facility (SSRF). The wavelength of the X-ray beam is 1.24 Å. The scattering vector q is defined as $q = 4\pi \sin \theta/\lambda$, where λ is the X-ray wavelength and 2θ is the scattering angle. Silver behenate was used for calibration. Differential scanning calorimetry (DSC) measurements were conducted on a DSC 2500 (TA Instruments) with a mechanical cooler. A controlled cooling at a

https://dx.doi.org/10.1021/acs.macromol.0c00158
Macromolecules XXXX, XXX, XXX−XXX

rate of 10 °C/min was always carried out first; subsequent heating was performed at a rate equal to that of the previous cooling.

Broad dielectric measurement was conducted on a Novocontrol Concept 40 system with Alpha-A impedance analyzer and Quatro Cryosystem temperature control with an accuracy of 0.1 K. The sample was dried in high vacuum at 50 °C for 3 days and placed between two round gold electrodes. A Teflon ring with a thickness of 54 μm was used as a spacer between the electrodes. The measurement frequency was in the range of 0.05−10^7 Hz. Rheological properties were determined on a Modular Compact Rheometer 302 (Anton Paar Instruments) with a cone plate (CP25-2; an angle of 2°, a diameter of 25 mm, and a gap of 0.106 mm). During the frequency sweep measurements, the samples were strained in the linear regime within 10% at the frequency range of 0.01−100 Hz.

2.3. Sample Preparation. *2.3.1. Synthesis of Poly(1, 2-butylene oxide).* The alkene-functionalized potassium alkoxide initiator and terminator were prepared according to the procedures reported.[52] The synthetic route of PBO is illustrated in Scheme 1a. PBO

Scheme 1. Synthetic Routes of (a) PBO via Oxy-Anionic Ring-Opening Polymerization and (b) POSS through the Corner-Capping Reaction

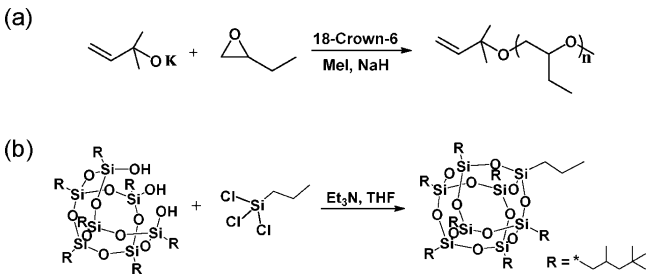

polymers with different molecular weights were synthesized via anionic ring-opening polymerization in accordance with the methods described previously.[53] Briefly, the catalyst 18-crown-6 was added into a flask and freeze-thawed three times. The initiator solution was added under a nitrogen atmosphere, and THF was then removed. The pre-dried BO monomer and toluene were distilled into the reactor. The reaction was maintained at 60 °C for at least 2 days. To terminate the reaction, sodium hydride and methyl iodide were added into the flask and the mixture was kept at room temperature for one more day. The resulting polymer was purified by extracting with dichloromethane and washed with water three times to yield a colorless viscous liquid. The PBO polymers with different molecular weights were denoted as PBO-*m*, where *m* represents the number-averaged molecular weight of the sample.

2.3.2. Synthesis of Propylhepta(isooctyl) POSS. The synthetic route of propylhepta(isooctyl) POSS is illustrated in Scheme 1b. Trisilanolisooctyl POSS (5.00 g, 4.22 mmol), triethylamine (3.81 mL, 27.45 mmol), and THF (32 mL) were added into a round-bottom flask under a nitrogen atmosphere. The reactor was kept at 0 °C, and trichloropropylsilane (1.25 mL, 8.44 mmol) in THF (14 mL) was slowly dropped into the mixture. Afterward, the solution was stirred overnight at room temperature. After the removal of triethylamine hydrochloride, the mixture was concentrated and purified by column chromatography using hexane as the eluent to yield a transparent and viscous product.

2.3.3. Preparation of PNCs. PBO and POSS in different compositions were dissolved in toluene at a concentration of 1 wt %. The resulting mixture was stirred for 12 h and was then dried in high vacuum at 50 °C for at least 3 days. The volume fraction of POSS was calculated by using the densities of POSS (1.01 g/cm^3; provided by Hybrid Plastics) and PBO (0.98 g/cm^3)[48] at room temperature and assuming the additivity of volumes. The resulting PNCs were denoted as POSS/PBO-*m*.

3. RESULTS

3.1. Synthesis and Chemical Characterization. A series of PBO samples of different molecular weights (M_n = 2.4k, 3.9k, 4.9k, 12.7k, and 39.0k) were synthesized via oxy-anionic ring-opening polymerization in toluene at 60 °C, as described in section 2. Molecular nanoparticle POSS in a form of transparent viscous liquid was obtained by adapting the corner-capping reaction. The synthetic routes are demonstrated in Scheme 1.

The chemical structures of PBO have been fully characterized by ^{1}H NMR, as shown in Figure 1a and Figure S1. All

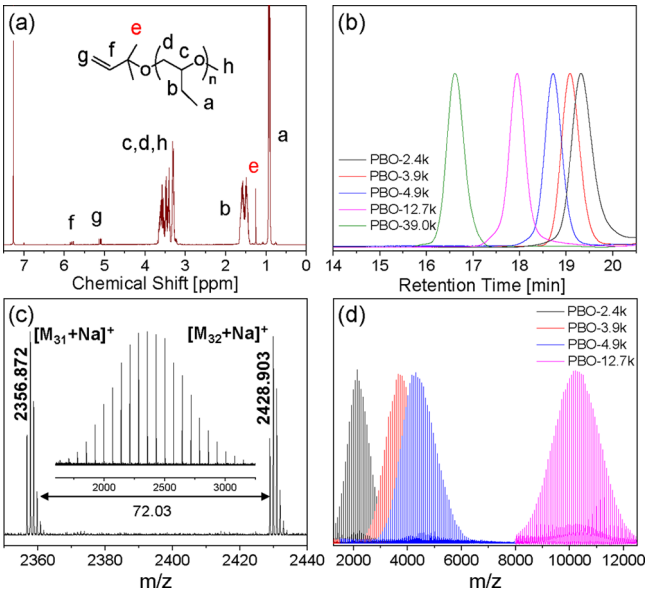

Figure 1. (a) Representative ^{1}H NMR spectrum of PBO-2.4k. (b) GPC chromatograms of PBO samples. (c) Representative high-resolution MALDI-TOF MS spectrum of PBO-2.4k. (d) MALDI-TOF MS spectra of PBO samples.

the resonances in the ^{1}H NMR spectrum can be identified. The characteristic resonances at 5.72−5.84 and 5.13−5.01 ppm correspond to the protons (f, g) on the double bond. The resonances at 1.24−1.20 ppm belong to the methyl groups (e) next to the double bond. The resonances at 3.68−3.10, 1.64−1.36, and 0.97−0.78 ppm correspond to the aliphatic protons (c, d, b, a) in the backbone. The molecular weight can be determined by calculating the integration ratio between the resonances of the end group and the backbone. The GPC chromatograms of PBO in Figure 1b exhibit symmetric and narrow monomodal peaks at different retention times. The molecular weights are consistent with the designed values, implying the living nature of the oxy-anionic polymerization free of side reactions or chain transfer in our experiments.

MALDI-TOF MS characterization has been performed to further identify the chemical structures of PBO samples including the end groups in more detail. As shown in Figure 1c,d, only one mass distribution composed of equal interval peaks has been observed in the spectrum, implying a well-defined chemical structure of the target polymer with discrete end groups and free of side reactions. The interval value (m/z = 72.03) between the neighboring peaks matches the mass of the repeat unit (m/z = 72.06) of PBO. The calculated exact mass of [M_{31}+Na] (m/z = 85.07 + 72.06 × 31 + 15.02 + 22.99 = 2356.94) in Figure 1c is consistent with the experimental

https://dx.doi.org/10.1021/acs.macromol.0c00158
Macromolecules XXXX, XXX, XXX−XXX

value (m/z = 2356.87), suggesting the success of the anionic polymerization with quantitative end functionalization. The sample information is summarized in Table 1.

Table 1. Characteristics of PBO Samples

sample	DP[a]	M_n[a] (kg·mol^{-1})	M_w[b] (kg·mol^{-1})	PDI[b]	Rg[c] (nm)
PBO-2.4k	32	2.4	2.6	1.07	1.4
PBO-3.9k	53	3.9	4.1	1.05	1.8
PBO-4.9k	66	4.9	5.1	1.04	2.0
PBO-12.7k	174	12.7	13.2	1.04	3.2
PBO-39.0k	540	39.0	41.3	1.06	5.6

[a]Determined by the ^{1}H NMR measurements. [b]Determined by the GPC measurements in THF. [c]Calculated according to $\langle R_{ee}^2\rangle_0/M_w$ = 0.49 Å^2·mol/g[54,55] under the Gaussian approximation,[56] $\langle R_{ee}^2\rangle_0$ is the mean-square end-to-end distance of an unperturbed chain. The Kuhn length of PBO is estimated to be 0.79 nm.[54]

The chemical structure of POSS has been characterized by ^{1}H NMR, as shown in Figure 2a. All the resonances in the ^{1}H

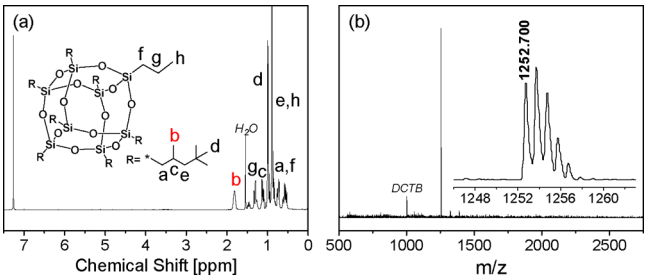

Figure 2. (a) ^{1}H NMR spectrum and (b) MALDI-TOF MS spectrum of POSS.

NMR spectrum can be identified. The success of the synthesis was further confirmed by the MALDI-TOF MS spectrum, as seen in Figure 2b. The sharp signal at m/z = 1252.70 is consistent with the calculated mass (m/z = 1251.75) according to the formula $[C_{59}H_{126}O_{12}Si_8+H]^+$.

3.2. Dispersion of POSS in the PBO Matrix. To evaluate the miscibility between POSS and the PBO matrix, their solubility parameters were first estimated and comparison was made consequently. A small difference between the solubility parameters generally indicates good compatibility. The theoretical solubility parameter (δ, also called Hildebrand parameter) is defined as the square root of the cohesive energy density.[57] Capitalizing on the group contribution method, the solubility parameter δ has been evaluated as follows:

$$\delta = \frac{\sum F}{\bar{V}} = \frac{\rho \sum F}{M} \quad (1)$$

where ρ, F, and M are the density, the molar attraction constant, and the molecular weight of the repeat unit of the polymer, respectively. The δ of PBO was calculated as 8.30 (cal/cm^3)$^{1/2}$ by using the F values from literature.[57,58] For POSS (MW = 1322.476 g/mol), most of the F values were adopted from the literature as well,[58] except that of the Si−O group, which was estimated as 275.77 (cal·cm^3)$^{1/2}$·mol^{-1} by referring to the experimental solubility parameter of poly(dimethylsiloxane) (ρ = 0.98 g/cm^3 and MW = 74 g/mol).[59] Accordingly, the δ of POSS was estimated as 8.40 (cal/cm^3)$^{1/2}$, close to that of PBO. The very small difference between the estimated solubility parameters suggests good compatibility of POSS with the PBO matrix in our PNC system and an athermal interaction in nature. The solubility parameters are included in Table 2.

Table 2. Theoretical Solubility Parameter Values of POSS and PBO

sample	ΣF ((cal·cm^3)$^{1/2}$·mol^{-1})	ρ (g·cm^{-3})	MW (g·mol^{-1})	δ ((cal·cm^{-3})$^{1/2}$)
POSS	10409.9	1.01	1252.33	8.40
BO	612.3	0.98	72.11	8.32

The dispersity of POSS in the PBO matrix as a function of its content was investigated experimentally by WAXD measurements. As shown in Figure 3, the neat POSS molecular

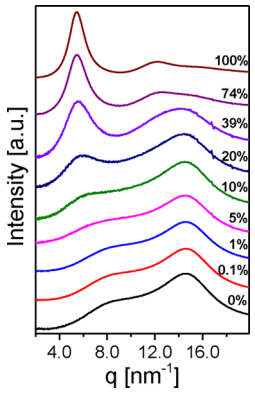

Figure 3. 1D X-ray diffraction profiles of POSS/PBO-12.7k mixtures as a function of the volume fraction of POSS.

nanoparticles in close packing exhibit a characteristic scattering around $q \sim 5.4$ nm^{-1}, which has been used as the sign of aggregation of POSS. As the volume fraction of POSS is ≤10 vol %, no apparent sign of aggregation of POSS is present in the scattering profiles of the POSS/PBO PNCs, as also shown in Figure S2 for PBO of different molecular weights. When the volume fraction of POSS is ≥20 vol %, the characteristic scattering of POSS aggregates becomes distinct, indicating obvious aggregation or phase separation of POSS in the polymer matrix. The differential scattering profiles of the PNCs with respect to that of neat PBO are demonstrated in Figure S3 to resolve the subtle contribution of the scattering from POSS at different volume fractions. Nanoparticles that start to aggregate above a critical volume fraction has been also observed in a weakly attractive system in the simulation.[60] In this work, 10 vol % is taken as the critical value and only the PNCs at the volume fraction of POSS of ≤10 vol % will be discussed.

3.3. Dielectric Relaxation of PNCs. BDS has been utilized to investigate the hierarchical dielectric relaxations of the PNCs. As shown in Figure 4, simultaneous global chain dynamics and local segmental dynamics can be clearly identified. In the representative temperature-dependent dielectric spectra of POSS/PBO-3.9k at 5 vol %, two well-separated relaxation processes located at high- and low-frequency regimes in the imaginary part correspond to the segmental relaxation and the normal mode of chain relaxation, respectively. As the temperature decreases, these two relaxation processes shifted to a lower frequency. The dielectric spectra of

https://dx.doi.org/10.1021/acs.macromol.0c00158
Macromolecules XXXX, XXX, XXX−XXX

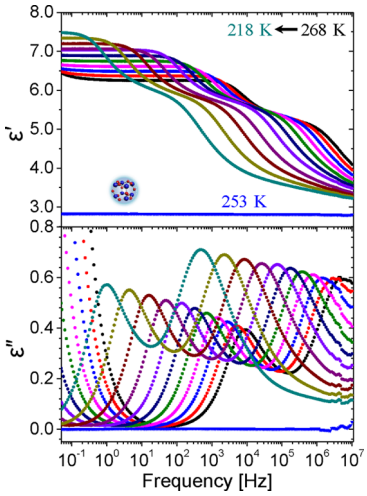

Figure 4. Dielectric spectra of POSS/PBO-3.9k at 5 vol %, with the real part ε' (top) and the imaginary part ε'' (bottom) as a function of temperature from 268 to 218 K in a step of 5 K. The nearly flat blue lines are the dielectric spectra of neat POSS at 253 K.

neat POSS are also included in Figure 4. A nearly flat line without involvement of any relaxation processes is observed in the bottom of the imaginary dielectric spectrum, which can be ascribed to the rigid and symmetric nature of POSS molecular nanoparticles. Remarkably, this dielectric "invisibility" of POSS in the composite systems is of a great advantage to selectively probe the dynamics of the host polymer PBO.

The representative dielectric spectra of POSS/PBO PNCs comprising PBO of different molecular weights at different volume fractions of POSS are shown in Figure 5a. The imaginary parts of permittivity normalized by the strength of

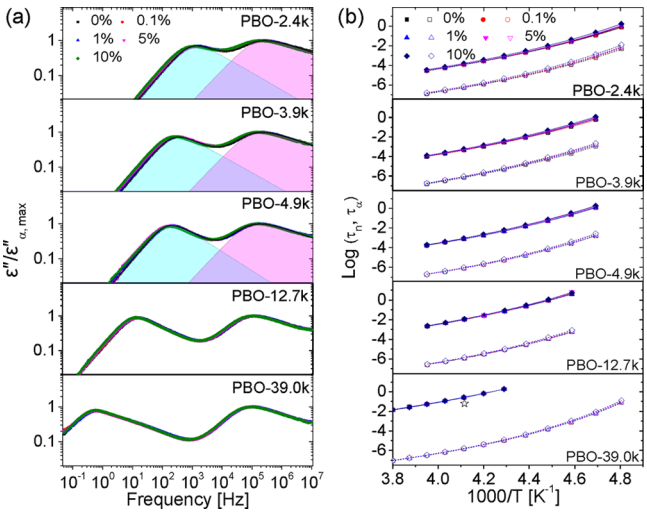

Figure 5. (a) Double-logarithmic plots of the normalized imaginary permittivity of POSS/PBO PNCs at different volume factions of POSS as a function of frequency at 243 K with the conductivity subtracted except the PNCs in PBO-39.0k; the molecular weights of PBO are 2.4k, 3.9k, 4.9k, 12.7k, and 39.0k from the top to the bottom. (b) Temperature dependence of relaxation time of the NM and the segmental mode in POSS/PBO PNCs. The solid symbols correspond to the NM relaxation, and the open symbols correspond to the segmental relaxation. The lines are the fittings according to the VFT equation. The open star indicates the terminal relaxation time of PBO-39.0k from the rheology measurements.

the segmental relaxation are plotted as a function of frequency at 243 K. The strong chain length dependence of the relaxation process at the low-frequency regime is characteristic of the NM of chain relaxation,[47,48] distinct from the behaviors of the segmental relaxation at the high-frequency regime. It is shown that the NM relaxation strengths of the PNCs at the volume fractions of POSS from 0.1 to 10 vol % remain almost constant with respect to that of the neat polymer. Meanwhile, a small increase in the relaxation time of the NM and the segmental mode with the volume fraction of POSS is observed. However, this tendency weakens with an increase in the molecular weight of PBO, as also shown in Figure S4.

The complex dielectric permittivity of the relaxation can be fitted by using the general Havriliak−Negami (HN) function as shown below:[39]

$$\varepsilon^* = \varepsilon_\infty + \frac{\Delta\varepsilon}{(1 + (i\omega\tau_{HN})^\beta)^\gamma} \quad (2)$$

where the parameter ε_∞ is the dielectric permittivity at the high-frequency limit, $\Delta\varepsilon$ is the relaxation strength, and τ_{HN} is the relaxation time. The exponents $0 < \beta, \beta\gamma \leq 1$ are the shape parameters, describing the symmetric and asymmetric broadening of the complex dielectric function. In the present case, a superposition of two HN functions and an additional conductivity term ($\sigma/i\varepsilon_0\omega$, ε_0 is the permittivity of vacuum) for dc conductivity were used. The well-separated relaxation processes and the simultaneous fitting with the real and imaginary parts facilitate to determine the characteristic relaxation times. It has been shown that the HN function can be usually used for fitting the dielectric chain relaxation of short chains when the low p modes in the discrete Rouse model are particularly interested,[39,43] while the segmental dynamics may overlap significantly with the high-frequency components of the Rouse chain dynamics.[29] Fits of the dielectric spectra of some neat polymers are also shown in Figure 5a, where the fits in the black solid lines coincide with experimental data in solid symbols very well. The relaxation time corresponding to the maximum dielectric loss was calculated according to

$$\tau_{max} = \tau_{HN}\left(\sin\frac{\beta\pi}{2(1+\gamma)}\right)^{-1/\beta}\left(\sin\frac{\beta\gamma\pi}{2(1+\gamma)}\right)^{1/\beta} \quad (3)$$

For the systems comprising polymers PBO-12.7k and PBO-39.0k, no fitting was applied and the characteristic relaxation time τ_{max} ($\tau_{max} = 1/2\pi f_{max}$) at the peak position f_{max} was directly used, considering the hierarchical relaxation processes involved in the dynamics of entangled polymer chains.[29,43,61] τ_{max} can be utilized as the longest relaxation time especially for the dielectric mode immediately followed by the low-frequency terminal tail in the monodispersed polymers.[43] Their dielectric relaxation spectra are directly used for the comparison.

Figure 5b represents the Arrhenius plots of the relaxation time of the segmental and the chain relaxation of systems of different polymer chain lengths at different volume fractions of POSS. As shown in Figure 5b, the temperature dependence of the chain and the segmental relaxation time can be well described by the Vogel−Fulcher−Tammann (VFT) equation[39]

$$\tau = \tau_0 \exp\left(\frac{DT_0}{T - T_0}\right) \quad (4)$$

https://dx.doi.org/10.1021/acs.macromol.0c00158
Macromolecules XXXX, XXX, XXX−XXX

where τ_0 is the relaxation time at an infinitely high temperature, T_0 is the so-called Vogel temperature, D is the parameter related to fragility of the material. All the data have been well-fitted, and the fitting parameters are listed in Table S1. With an increase in the volume fraction of POSS, the NM and the segmental relaxation processes become slow and deviate more from the neat polymers at lower temperatures. This effect is more pronounced for PBO of low molecular weight, while it becomes weak and nearly vanishes with an increase in the polymer chain length. This has been further testified by using DSC measurements. As shown in Figure S5a, the calorimetric glass transition temperature of PBO-4.9k is found to increase with the addition of POSS, while that of PBO-39.0k is nearly unaltered. The dielectric glass transition temperature can be also estimated by extrapolation of the dielectric segmental relaxation time in the VFT plots to 100 s, as demonstrated in Figure S5b, which is consistent with the calorimetric glass transition temperature and shows a similar behavior. The effect of the non-sticky nanoparticles on the segmental relaxation of the polymer matrix or its glass transition is speculated to be related to the impart of POSS on the excess free volume from the polymer chain ends, which will be further discussed in the following section.

PBO is a typical type-A polymer, which enables us to extract the chain dimension from the dielectric strength of the NM relaxation. Because the static correlation of the end-to-end vectors among different polymers on the global chain length scale can be neglected, the Onsager equation is applicable to the NM relaxation:[39]

$$\Delta\varepsilon_n = \frac{4\pi N_A \mu_p^2 F_{onsager}}{3M_W k_B T}\langle R_{ee}^2\rangle \tag{5}$$

where N_A is the Avogadro's constant, μ_p is the magnitude of monomeric dipole moment along the PBO chain contour ($\sim 1.65 \times 10^{-11}$ esu),[47] M_w is the weight-averaged molecular weight of the polymer, $\langle R_{ee}^2\rangle$ is the mean-square end-to-end distance of the polymer chain, and $F_{onsager}$ is a correction factor for the difference in the strengths of macroscopic and microscopic electric fields. $F_{onsager} \approx 1$ for the global chain dynamics, as the end-to-end vector relaxation of the chain, is on a much larger spatial scale than the size of the segment.[42,43] The dielectric strength $\Delta\varepsilon_n$ due to the global chain motion is thus directly related to $\langle R_{ee}^2\rangle$. Equation 5 has been utilized to analyze the change of the chain dimension through the relative change of the dielectric strength, as shown in Figure 5a.

Figure 6 depicts the relative change of the mean-square end-to-end distance of polymer chain in PNCs in comparison with that of the neat polymer as a function of volume fraction of POSS in PBO of different molecular weights. It shows a negligible change in the chain dimension, independent of volume fraction of POSS and polymer chain length. For the entangled PBO-39.0k samples, the dielectric spectra at different volume fractions of POSS coincide with each other well, which strongly suggests almost no impart of the introduction of POSS on the chain dimension of PBO and its hierarchical dynamics as well.

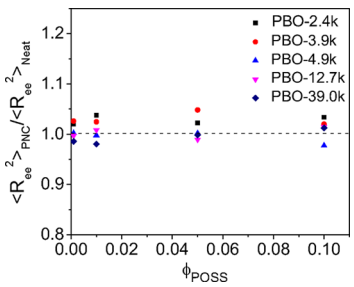

Figure 6. Plot of the ratio of the mean-square end-to-end distance of PBO in PNCs to that in the neat state as a function of volume fraction of POSS in PBO of different chain lengths.

3.4. Rheology of PNCs. Figure 7 shows the master curves for the storage moduli (G') and the loss moduli (G'') of PBO-4.9k and PBO-39.0k and their PNCs at 5 vol % as a function of shear rate, which were constructed by the time−temperature superposition at the reference temperature of 243 K with a horizontal shift factor α_T. For PBO-39.0k samples, an emergence of the elastic plateau in the storage modulus indicates entanglement of PBO chains. The entanglement molecular weight, M_e, can be estimated from the rubbery plateau as follows:[62]

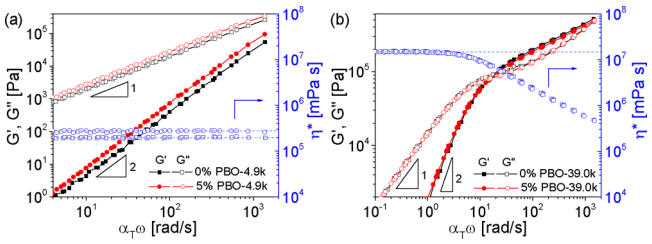

Figure 7. Rheological master curves of PNCs constructed by time−temperature superposition for (a) PBO-4.9k and (b) PBO-39.0k as a function of shear rate at T_{ref} = 243 K. The terminal relaxation time of PBO-39.0k is extracted from the crossover point of G' (solid symbol) and G'' (open symbol). Both spectra illustrate characteristic terminal relaxation behaviors. The zero-shear viscosities of the PNCs (blue open square) and the neat polymer (blue open circle) were determined by the plateau of the complex viscosity at a low angular frequency.

$$G_N^0 = \frac{4\rho RT}{5M_e} \tag{6}$$

where G_N^0 is the plateau modulus, ρ is the density of the host polymer, R is the gas constant, and T is the Kelvin temperature. The storage modulus at the minimum of loss factor tan δ was chosen as the plateau modulus. The M_e of PBO was thus estimated to be 8500 g/mol, as shown in Figure S6, which is consistent with the critical molecular weight determined from the molecular weight dependence of the dielectric chain relaxation time in Figure S7. This value is also in agreement with that of (8800 ± 1100) g/mol reported in the literature.[29] Therefore, PBO-4.9k is unentangled and PBO-39.0 k is weakly entangled. Both polymers exhibit characteristic terminal relaxation with the introduction of POSS, where $G' \approx \omega^2$ and $G'' \approx \omega$.[1] This Newtonian behavior also suggests the generally good dispersion of POSS in the PBO matrix at low volume fractions. In Figure 7b, the terminal relaxation time relevant to the disentangle time was determined through the crossover angular frequency of G' and G''. By comparing the entangled polymer and its PNC, no significant changes in moduli and relaxation time were observed. For PBO-4.9k melt and its PNC, the viscosities are comparably low. Nevertheless, the small shift of the terminal relaxation time to a low-

https://dx.doi.org/10.1021/acs.macromol.0c00158
Macromolecules XXXX, XXX, XXX−XXX

frequency regime with the introduction of POSS still can be deduced, which is consistent with the dielectric NM relaxation results. No significant changes in the rubbery plateau, terminal relaxation time, and power law of G' and G'' *versus* ω with POSS up to 5 vol % indicate negligible effects of POSS on the entanglement and terminal relaxation in rheology, which is also consistent with the dielectric chain relaxation illustrated in Figure 5b. The discrepancy between the dielectric and viscoelastic relaxation times shown in Figure 5b can be ascribed to the fundamental differences between the correlations involved in relaxation; thus, in dielectrics, only odd modes are relevant in contrast to rheology where all modes contribute.[29,42,43,61] As also demonstrated in Figure 7, the zero-shear viscosity of PBO-4.9k slightly increases with addition of POSS, while nearly no change can be observed for PBO-39.0k systems, which is consistent with the effects of POSS on the terminal relaxations of the polymers.

4. DISCUSSIONS

4.1. Effects of Nanoparticles on the Chain Dimension.

Our experiments clearly show that the mean-square end-to-end distance of the polymer chains derived from the dielectric strength of the NM relaxation remains identical with that of the neat polymer (in our case, Rg > R_N), independent of the POSS volume fraction (up to 10 vol %) and the chain length. It has been argued that the chain dimension in PNCs is dependent on the sign of the interaction between the nanoparticle and polymer[16,18,24] and the relative size of the chain with respect to the nanoparticle.[5,13−15]

The excluded volume effect of nanoparticles as a good solvent in "polymer-in-nanoparticle" solution was proposed to account for chain expansion in PNCs. This argument has been supported by the simulation and neutron scattering (NS) experiments, for example, in the athermal cross-linked PS nanoparticles/PS system[5,13,20] and trimethylsilyl-treated poly-silica/PDMS system,[21] especially when the size of the nanoparticle is smaller than that of the polymer. The solvent effect of nanoparticles on chain swelling was argued in a recent work,[63] where if PNCs could be regarded as polymer-in-nanoparticle solution, the chain dimension should be independent of the polymer volume fraction in the concentrated regime due to the screening effect of polymers. For typical well-dispersed PNCs as mentioned above, the concentration of nanoparticles in the good dispersion state is usually less than 20 vol %; therefore, the polymers should still be in the concentrated regime, and an ideal chain statistics should be adapted. The presence of nanoparticles would not be able to influence the chain dimension significantly. This argument seems consistent with some experimental results, for example, in the miscible phenyl coating silica/PS nano-composite system,[15] pentyl-coated SiO_2/PS,[14,17,22,23] and PEO-grafted POSS in the PEO matrix.[64]

In our non-sticky athermal system, the unaltered chain dimension with introduction of nanoparticles is observed, consistent with above arguments regarding the screened excluded volume effects. In our PNCs, the concentration of the polymer is larger than 90 vol %, far beyond the critical overlapping concentration of polymers in the concentrated regime if POSS was treated as a regular solvent molecule. It is worth noting that other aspects such as the particle size compared to the statistic segmental length or Kuhn length of the polymer and its immobility may need to be considered as well. In a thermodynamic point of view, the polymer chain conforms to a random-walk and phantom chain statistics while requires a nearly constant and uniform mass density. The short-range interference on the immediate segment scale is so large that the effects in the long range can be totally screened out as the result of the many-chain statistics of the polymer melt; the de Gennes "blob" size is reduced to that of the statistical segment.[65] Meanwhile, due to the decoupling of different x, y, z components of an ideal chain's random walk,[56,65] constraint in one dimension would not necessarily perturb the conformation of an ideal chain in other dimensions. Recently, the unperturbed Gaussian statistics of polymer chains upon mixing with nanoparticles was verified by NS measurements in the intermediate-to-high q region.[16,64] A negligible change of the mean-square end-to-end distance of the polymer melt in neutral diblock copolymer single-crystal platelets has been also observed experimentally.[51] Interestingly, the lattice Monte Carlo simulation demonstrated the unaffected overall Gaussian chain statistics regardless of the filler loading up to 27 vol %, despite the complex structures in the vicinity of the nanoparticle at the subchain level.[22] We think that it is the peculiar property of the polymer melt that results in the unaffected end-to-end chain dimension, particularly manifested in PNCs.

4.2. Effects of Nanoparticles on Hierarchical Dynamics of Host Polymers in PNCs.

4.2.1. Confinement Effect. In PNCs, the hierarchical dynamics of polymers confined between nanoparticles is essential to understand the physical properties of nanocomposites and their performance enhancement. The confinement parameter (defined as ID/2Rg, where ID is the interfacial surface-to-surface distance) has been widely employed to evaluate the confinement effects of nanoparticles on relevant length scales.[32,34] The ID between spherical nanoparticles in PNCs can be estimated as follows:

$$\mathrm{ID} = d_N\left(\left(\frac{\varphi_N^M}{\varphi_N}\right)^{1/3} - 1\right) \tag{7}$$

where φ_N^M, φ_N, and d_N represent the maximum volume fraction, the volume fraction, and the diameter of nanoparticles, respectively. Here, φ_N^M is equal to 0.637 by assuming random close packing (RCP) of nanoparticles[32,34] and ID represents the nearest distance between the surfaces of neighboring nanoparticles. The mean diameter of POSS (d_N) can be estimated as

$$d_N = 2 \times \left(\frac{3M_{POSS}\varphi_N^M}{4N_A\pi\rho_{POSS}}\right)^{1/3} \tag{8}$$

where M_{POSS}, ρ_{POSS}, and N_A represent the molecular weight, the bulk density of POSS, and the Avogadro's constant, respectively. The calculated ID/2Rg are listed in Table S2.

Figure 8a shows the reduced dielectric chain relaxation time of PBO in PNCs as a function of ID/2Rg. As shown in the figure, the reduced dielectric chain relaxation time generally starts to increase on the order of ID/2Rg close to unity and does not collapse onto each other. As the chain length increases, the chain relaxation time upturns at a comparably lower confinement parameter or under higher confinement. There appears no universal turning point for the confinement of the chain dynamics at different chain lengths.

As shown in Figure 5, both the chain and segmental relaxation time slow down simultaneously with addition of

https://dx.doi.org/10.1021/acs.macromol.0c00158
Macromolecules XXXX, XXX, XXX−XXX

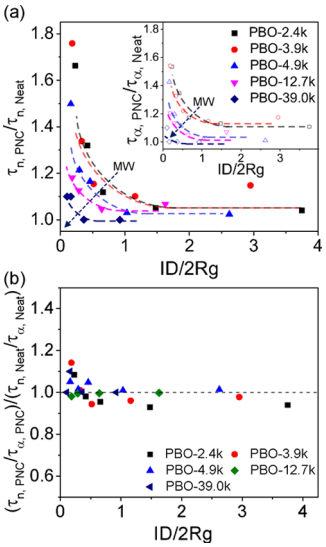

Figure 8. (a) Reduced dielectric chain relaxation time by that of the neat polymer and (b) reduced dielectric chain relaxation time by the reduced segmental relaxation time with respect to the neat polymer *versus* confinement parameter (ID/2Rg) in POSS/PBO systems at 243 K. The inset of (a) is the reduced segmental relaxation time *versus* ID/2Rg. The arrow directs the increase in molecular weight. The dashed line is a guide for the eyes.

POSS and exhibit a similar temperature dependence. The deviation of the relaxation time from that of the neat polymer is more pronounced for the short chains as the temperature decreases and approaches the glass transition temperature, while this deviation is negligible for the long polymer chains. The inset of Figure 8a represents the reduced segmental relaxation time *versus* confinement parameters, wherein a very similar trend as that of chain relaxation is observed, suggesting a possible correlation between the chain relaxation and the segmental relaxation. To explicitly explore the relationship between the confined chain relaxation and the segmental relaxation, the chain relaxation time is normalized by the segmental relaxation time, as shown in Figure 8b. Indeed, the reduced chain relaxation times with respect to different confinement parameters can be more or less collapsed with a nearly constant tendency when normalized by the reduced segmental relaxation time, regardless of the chain length and the POSS volume fraction. This suggests that the confinements on the chain dynamics and segmental dynamics should be correlated; in other words, the confinement on the global chain dynamics should be related to the influenced local segmental dynamics by the nanoparticles. For our athermal system, POSS has no enthalpic interaction with PBO. The slowing down of the segmental relaxation cannot be attributed to the attractive interaction between POSS and the polymer segments. The chain length dependence on the segmental relaxation points to the chain end effect, which is typically observed in the molecular weight dependence on the glass transition temperature.[66,67] Herein, the addition of nanoparticles may affect more on the short chains with more fractions of chain ends as also elucidated by the calorimetric glass transition behaviors shown in Figure S5, and their excess free volume may be reduced when in contact with comparably immobile nanoparticles. The correlation between the chain dynamics and the segmental dynamics is understandable since the chain dynamics is essentially relevant to the segmental dynamics and monomer friction. It is worth noting that, for NM relaxation, the $p = 1$ mode associated with the end-to-end vector fluctuation is probed, in contrast to the center-of-mass diffusion of the $p = 0$ mode.[32,35]

4.2.2. Solvent Effect. Solvents can affect the thermodynamics of polymer solution and its dynamics as well. As shown before, the addition of nanoparticles up to 10 vol % is not enough to change the chain dimension in the PNCs because the system should still be in the concentrated regime. However, such an amount of solvent is expected to have a dramatic effect on the dynamics of the polymer solution due to the so-called plasticizer effect, which has been widely applied to modify the viscoelastic or mechanical properties of polymers.[68] Usually, a very small amount of molecularly dispersed plasticizer can sharply reduce the local friction coefficient of polymer segments so as to impose a big impact on the dynamics of polymers. In our system, we observed the slowing down of the segment as well as the chain dynamics of the host polymers especially for the short chains as the nanoparticles were added, strongly suggesting that the size of POSS (~8 times of the Kuhn segment of PBO in volume) and its relative immobility should have played distinct roles on the polymer dynamics.

4.2.3. Filler Effect. Fillers are widely applied to improve the properties such as mechanic strength and flow behavior of polymers.[6,8,69−78] Considering the hierarchical structures and dynamics of polymers and the impacts of nanoparticles on the different length and time scales, the composite system is much complicated. The classical hydrodynamic description of continuum medium often fails especially for relatively small nanoparticles.[79]

For entangled polymers, the tube size is a characteristic length scale for the polymer chains starting to entangle topologically. When small nanoparticles are introduced, it is argued that disentanglement could take place due to volume occupation by the nanoparticles. Especially when the size of the nanoparticle was smaller than the tube size, tube dilation was observed, e.g., in the NS experiments and simulation,[30,31,80,81] which could further result in accelerated dynamics and decreased viscosity of the nanocomposites particularly below a critical concentration of nanoparticles. In order to have a pronounced topological disentanglement phenomenon, the volume of the nanoparticles is usually high (e.g., ~20% dependent on the relative size of nanoparticles and the tube size).[80,82] For long polymer chains, the geometrical constraint from the nanoparticles may also confine the chain dynamics, acting like fixed obstacles to decrease the tube size.[30,31] The overall effects of the nanoparticles on the reptation dynamics of the entangled chains are thus speculated to result from the balance between these two competitive contributions on the topology aspect. Either decrease or reinforcement of the viscosity of the nanocomposite has been also argued in terms of the possible existence of a layer of reduced local viscosity surrounding the nanoparticles, which eventually results in different rheological behaviors of PNCs as a whole.[5,70,83−85] Our experiments on the dielectric chain relaxation in the athermal PNCs illustrate essentially no change of the NM chain relaxation at the isofrictional state on the scale of the segment and the rheological terminal relaxation at a relatively low volume fraction of well-dispersed non-sticky small nanoparticles.

https://dx.doi.org/10.1021/acs.macromol.0c00158
Macromolecules XXXX, XXX, XXX−XXX

5. CONCLUSIONS

We have designed and synthesized a series of well-defined PBO of different chain lengths as well as non-crystalline molecular nanoparticle POSS to construct non-sticky PNC mode systems. The dispersity of POSS in the PBO matrix has been estimated by the solubility parameters and investigated by the WAXD experiments. The type-A nature of PBO and dielectric "invisibility" of POSS molecular nanoparticles enable to exclusively probe the chain dimension and hierarchical dynamics of polymers in the PNCs by utilizing BDS. The effects of addition of POSS into PBO in the unentangled and the entangled regions have been systematically investigated by combining BDS and rheology experiments. We observed no change in the chain dimension derived from the relative strength of the dielectric NM relaxation, independent of the volume fraction of the nanoparticles and the polymer chain lengths. This has been ascribed to the peculiar properties of the polymer melt with screened excluded volume effect, particularly in the concentrated region. The slowing down of the dielectric chain relaxation and segmental relaxation under strong confinement (ID/2Rg < 1) was observed especially for the short polymer chains, which has been considered to originate from the impart of the nanoparticles on the polymer chain ends. After renormalizing with the segmental relaxation, the change of chain dynamics as a function of confinement parameters can be barely observed with respect to the neat polymers, which is also consistent with the rheological results. The small nanoparticles affect the hierarchical structures and dynamics of polymers on different length and time scales in a comprehensive way, distinct from the regular plasticizer effect and eventually leading to the unchanged overall chain dynamics in the athermal PNCs especially at a relatively low filler content.

■ ASSOCIATED CONTENT

Supporting Information

The Supporting Information is available free of charge at https://pubs.acs.org/doi/10.1021/acs.macromol.0c00158.

Chemical characterization, confinement parameters, rheological and DSC characterization, and fitting parameters (PDF)

■ AUTHOR INFORMATION

Corresponding Author

Huiming Xiong − *Department of Polymer Science, School of Chemistry and Chemical Engineering, Frontiers Science Center for Transformative Molecules, Center for Soft Matter and Interdisciplinary Sciences, Shanghai Jiao Tong University, Shanghai 200240, P. R. China*; orcid.org/0000-0001-6628-8519; Email: hmxiong@sjtu.edu.cn

Authors

Xinlin Zhang − *Department of Polymer Science, School of Chemistry and Chemical Engineering, Frontiers Science Center for Transformative Molecules, Center for Soft Matter and Interdisciplinary Sciences, Shanghai Jiao Tong University, Shanghai 200240, P. R. China*

Wei Wei − *Department of Polymer Science, School of Chemistry and Chemical Engineering, Frontiers Science Center for Transformative Molecules, Center for Soft Matter and Interdisciplinary Sciences, Shanghai Jiao Tong University, Shanghai 200240, P. R. China*

Xin Jin − *Department of Polymer Science, School of Chemistry and Chemical Engineering, Frontiers Science Center for Transformative Molecules, Center for Soft Matter and Interdisciplinary Sciences, Shanghai Jiao Tong University, Shanghai 200240, P. R. China*

Complete contact information is available at: https://pubs.acs.org/10.1021/acs.macromol.0c00158

Notes

The authors declare no competing financial interest.

■ ACKNOWLEDGMENTS

This research is supported by the National Natural Science Foundation of China (nos. 21790345 and 21574082). We appreciate the use of the BL14B and BL16B beamlines in the Shanghai Synchrotron Radiation Facility (SSRF).

■ REFERENCES

(1) Kumar, S. K.; Benicewicz, B. C.; Vaia, R. A.; Winey, K. I. 50th Anniversary Perspective: Are Polymer Nanocomposites Practical for Applications? *Macromolecules* **2017**, *50*, 714−731.

(2) Jancar, J.; Douglas, J. F.; Starr, F. W.; Kumar, S. K.; Cassagnau, P.; Lesser, A. J.; Sternstein, S. S.; Buehler, M. J. Current Issues in Research on Structure-property Relationships in Polymer Nanocomposites. *Polymer* **2010**, *51*, 3321−3343.

(3) Kumar, S. K.; Ganesan, V.; Riggleman, R. A. Perspective: Outstanding Theoretical Questions in Polymer-nanoparticle Hybrids. *J. Chem. Phys.* **2017**, *147*, No. 020901.

(4) Karatrantos, A.; Composto, R. J.; Winey, K. I.; Kröger, M.; Clarke, N. Modeling of Entangled Polymer Diffusion in Melts and Nanocomposites: A Review. *Polymer* **2019**, *11*, 876.

(5) Mackay, M. E.; Tuteja, A.; Duxbury, P. M.; Hawker, C. J.; Van Horn, B.; Guan, Z.; Chen, G.; Krishnan, R. General Strategies for Nanoparticle Dispersion. *Science* **2006**, *311*, 1740−1743.

(6) Leblanc, J. L. Rubber-filler Interactions and Rheological Properties in Filled Compounds. *Prog. Polym. Sci.* **2002**, *27*, 627−687.

(7) Ray, S. S.; Okamoto, M. Polymer/layered Silicate Nanocomposites: A Review from Preparation to Processing. *Prog. Polym. Sci.* **2003**, *28*, 1539−1641.

(8) Giannelis, E. P.; Krishnamoorti, R.; Manias, E. Polymer-silicate Nanocomposites: Model Systems for Confined Polymers and Polymer Brushes. In *Polymers in confined environments*, Springer: 1999; pp. 107−147.

(9) Bačová, P.; Lo Verso, F.; Arbe, A.; Colmenero, J.; Pomposo, J. A.; Moreno, A. J. The Role of the Topological Constraints in the Chain Dynamics in All-polymer Nanocomposites. *Macromolecules* **2017**, *50*, 1719−1731.

(10) Martin, H. J.; White, B. T.; Yuan, G.; Saito, T.; Dadmun, M. D. Relative Size of the Polymer and Nanoparticle Controls Polymer Diffusion in All-polymer Nanocomposites. *Macromolecules* **2019**, *52*, 2843−2852.

(11) Kim, H.; Abdala, A. A.; Macosko, C. W. Graphene/Polymer Nanocomposites. *Macromolecules* **2010**, *43*, 6515−6530.

(12) Schneider, G. J. Dynamics of Nanocomposites. *Curr. Opin. Chem. Eng.* **2017**, *16*, 65−77.

(13) Tuteja, A.; Duxbury, P. M.; Mackay, M. E. Polymer Chain Swelling Induced by Dispersed Nanoparticles. *Phys. Rev. Lett.* **2008**, *100*, No. 077801.

(14) Sen, S.; Xie, Y.; Kumar, S. K.; Yang, H.; Bansal, A.; Ho, D. L.; Hall, L.; Hooper, J. B.; Schweizer, K. S. Chain Conformations and Bound-layer Correlations in Polymer Nanocomposites. *Phys. Rev. Lett.* **2007**, *98*, 128302.

(15) Crawford, M. K.; Smalley, R. J.; Cohen, G.; Hogan, B.; Wood, B.; Kumar, S. K.; Melnichenko, Y. B.; He, L.; Guise, W.; Hammouda, B. Chain Conformation in Polymer Nanocomposites with Uniformly Dispersed Nanoparticles. *Phys. Rev. Lett.* **2013**, *110*, 196001.

(16) Nusser, K.; Neueder, S.; Schneider, G. J.; Meyer, M.; Pyckhout-Hintzen, W.; Willner, L.; Radulescu, A.; Richter, D. Conformations of Silica-poly(ethylene-propylene) Nanocomposites. *Macromolecules* **2010**, *43*, 9837−9847.

(17) Jouault, N.; Dalmas, F.; Said, S.; Di Cola, E.; Schweins, R.; Jestin, J.; Boué, F. Direct Measurement of Polymer Chain Conformation in Well-controlled Model Nanocomposites by Combining SANS and SAXS. *Macromolecules* **2010**, *43*, 9881−9891.

(18) Robbes, A. S.; Cousin, F.; Meneau, F.; Jestin, J. Melt Chain Conformation in Nanoparticles/Polymer Nanocomposites Elucidated by the SANS Extrapolation Method: Evidence of the Filler Contribution. *Macromolecules* **2018**, *51*, 2216−2226.

(19) Karatrantos, A.; Clarke, N.; Composto, R. J.; Winey, K. I. Polymer Conformations in Polymer Nanocomposites Containing Spherical Nanoparticles. *Soft Matter* **2015**, *11*, 382−388.

(20) Frischknecht, A. L.; McGarrity, E. S.; Mackay, M. E. Expanded Chain Dimensions in Polymer Melts with Nanoparticle Fillers. *J. Chem. Phys.* **2010**, *132*, 204901.

(21) Nakatani, A. I.; Chen, W.; Schmidt, R. G.; Gordon, G. V.; Han, C. C. Chain Dimensions in Polysilicate-filled Poly(dimethyl siloxane). *Polymer* **2001**, *42*, 3713−3722.

(22) Ozmusul, M. S.; Picu, C. R.; Sternstein, S. S.; Kumar, S. K. Lattice Monte Carlo Simulations of Chain Conformations in Polymer Nanocomposites. *Macromolecules* **2005**, *38*, 4495−4500.

(23) Jouault, N.; Jestin, J. Intra- and Interchain Correlations in Polymer Nanocomposites: A Small-Angle Neutron Scattering Extrapolation Method. *ACS Macro Lett.* **2016**, *5*, 1095−1099.

(24) Li, Y.; Kröger, M.; Liu, W. K. Dynamic Structure of Unentangled Polymer Chains in the Vicinity of Non-attractive Nanoparticles. *Soft Matter* **2014**, *10*, 1723−1737.

(25) Gong, S.; Chen, Q.; Moll, J. F.; Kumar, S. K.; Colby, R. H. Segmental Dynamics of Polymer Melts with Spherical Nanoparticles. *ACS Macro Lett.* **2014**, *3*, 773−777.

(26) Jouault, N.; Moll, J. F.; Meng, D.; Windsor, K.; Ramcharan, S.; Kearney, C.; Kumar, S. K. Bound Polymer Layer in Nanocomposites. *ACS Macro Lett.* **2013**, *2*, 371−374.

(27) Carroll, B.; Cheng, S.; Sokolov, A. P. Analyzing the Interfacial Layer Properties in Polymer Nanocomposites by Broadband Dielectric Spectroscopy. *Macromolecules* **2017**, *50*, 6149−6163.

(28) Richter, D.; Kruteva, M. Polymer Dynamics Under Confinement. *Soft Matter* **2019**, *15*, 7316−7349.

(29) Gerstl, C.; Schneider, G. J.; Pyckhout-Hintzen, W.; Allgaier, J.; Richter, D.; Alegría, A.; Colmenero, J. Segmental and Normal Mode Relaxation of Poly (alkylene oxide)s Studied by Dielectric Spectroscopy and Rheology. *Macromolecules* **2010**, *43*, 4968−4977.

(30) Schneider, G. J.; Nusser, K.; Willner, L.; Falus, P.; Richter, D. Dynamics of Entangled Chains in Polymer Nanocomposites. *Macromolecules* **2011**, *44*, 5857−5860.

(31) Nusser, K.; Schneider, G. J.; Richter, D. Microscopic Origin of the Terminal Relaxation Time in Polymer Nanocomposites: an Experimental Precedent. *Soft Matter* **2011**, *7*, 7988−7991.

(32) Gam, S.; Meth, J. S.; Zane, S. G.; Chi, C.; Wood, B. A.; Seitz, M. E.; Winey, K. I.; Clarke, N.; Composto, R. J. Macromolecular Diffusion in A Crowded Polymer Nanocomposite. *Macromolecules* **2011**, *44*, 3494−3501.

(33) Elmahdy, M. M.; Chrissopoulou, K.; Afratis, A.; Floudas, G.; Anastasiadis, S. H. Effect of Confinement on Polymer Segmental Motion and Ion Mobility in PEO/layered Silicate Nanocomposites. *Macromolecules* **2006**, *39*, 5170−5173.

(34) Gam, S.; Meth, J. S.; Zane, S. G.; Chi, C.; Wood, B. A.; Winey, K. I.; Clarke, N.; Composto, R. J. Polymer Diffusion in a Polymer Nanocomposite: Effect of Nanoparticle Size and Polydispersity. *Soft Matter* **2012**, *8*, 6512−6520.

(35) Lin, C. C.; Gam, S.; Meth, J. S.; Clarke, N.; Winey, K. I.; Composto, R. J. Do Attractive Polymer-Nanoparticle Interactions Retard Polymer Diffusion in Nanocomposites? *Macromolecules* **2013**, *46*, 4502−4509.

(36) Holt, A. P.; Sangoro, J. R.; Wang, Y.; Agapov, A. L.; Sokolov, A. P. Chain and Segmental Dynamics of Poly (2-vinylpyridine) Nanocomposites. *Macromolecules* **2013**, *46*, 4168−4173.

(37) Bogoslovov, R. B.; Roland, C. M.; Ellis, A. R.; Randall, A. M.; Robertson, C. G. Effect of Silica Nanoparticles on the Local Segmental Dynamics in Poly(vinyl acetate). *Macromolecules* **2008**, *41*, 1289−1296.

(38) Hao, N.; Böhning, M.; Schönhals, A. Dielectric Properties of Nanocomposites Based on Polystyrene and Polyhedral Oligomeric Phenethyl-silsesquioxanes. *Macromolecules* **2007**, *40*, 9672−9679.

(39) Kremer, F.; Schönhals, A. *Broadband Dielectric Spectroscopy*; Springer Science & Business Media, 2012.

(40) Stockmayer, W. H. Dielectric Dispersion in Solutions of Flexible Polymers. *Pure Appl. Chem.* **1967**, *15*, 539−554.

(41) Stockmayer, W. H.; Burke, J. J. Dielectric Dispersion in Branched Polypropylene Oxides. *Macromolecules* **1969**, *2*, 647−650.

(42) Adachi, K.; Kotaka, T. Dielectric Normal Mode Relaxation. *Prog. Polym. Sci.* **1993**, *18*, 585−622.

(43) Watanabe, H. Dielectric Relaxation of Type-A Polymers in Melts and Solutions. *Macromol. Rapid Commun.* **2001**, *22*, 127−175.

(44) Nicolai, T.; Floudas, G. Dynamics of Linear and Star Poly(oxypropylene) studied by Dielectric Spectroscopy and Rheology. *Macromolecules* **1998**, *31*, 2578−2585.

(45) Schönhals, A. Relation between Main and Normal Mode Relaxations for Polyisoprene Studied by Dielectric Spectroscopy. *Macromolecules* **1993**, *26*, 1309−1312.

(46) Ding, Y.; Pawlus, S.; Sokolov, A. P.; Douglas, J. F.; Karim, A.; Soles, C. L. Dielectric Spectroscopy Investigation of Relaxation in C60-Polyisoprene Nanocomposites. *Macromolecules* **2009**, *42*, 3201−3206.

(47) Yamane, M.; Hirose, Y.; Adachi, K. Dielectric Normal and Segmental Modes in Undiluted Poly(butylene oxide). *Macromolecules* **2005**, *38*, 9210−9215.

(48) Urakawa, O.; Yamane, M.; Tomie, S.; Inoue, T.; Shikata, T.; Adachi, K. Relationship between Global and Segmental Dynamics of Poly(butylene oxide) Studied by Broadband Dielectric Spectroscopy. *J. Chem. Phys.* **2018**, *148*, No. 034904.

(49) Casalini, R.; Roland, C. M. Temperature and Density Effects on the Local Segmental and Global Chain Dynamics of Poly-(oxybutylene). *Macromolecules* **2005**, *38*, 1779−1788.

(50) Kyritsis, A.; Pissis, P.; Mai, S. M.; Booth, C. Comparative Dielectric Studies of Segmental and Normal Mode Dynamics of Poly(oxybutylene) and Poly(oxyethylene)-poly(oxybutylene) Diblock Copolymers. *Macromolecules* **2000**, *33*, 4581−4595.

(51) Jin, X.; Wei, W.; Zhang, X.; Xiong, H. Statistics and Dynamics of Polymer Melt in Neutral Diblock Copolymer Single-Crystal Platelets. *J. Phys. Chem. Lett.* **2020**, *11*, 1081−1086.

(52) Wei, W.; Xu, Z.; Xu, L.; Zhang, X.; Xiong, H.; Yang, J. Flexible Ionic Conducting Elastomers for All-Solid-State Room-Temperature Lithium Batteries. *ACS Appl. Energy Mater.* **2018**, *1*, 6769−6773.

(53) Liu, Y.; Wei, W.; Xiong, H. Gradient and Block Side-Chain Liquid Crystalline Polyethers. *Polym. Chem.* **2015**, *6*, 583−590.

(54) Gerstl, C.; Schneider, G. J.; Pyckhout-Hintzen, W.; Allgaier, J.; Willbold, S.; Hofmann, D.; Disko, U.; Frielinghaus, H.; Richter, D. Chain Conformation of Poly(alkylene oxide)s Studied by Small-Angle Neutron Scattering. *Macromolecules* **2011**, *44*, 6077−6084.

(55) Booth, C.; Orme, R. Unperturbed Dimensions of Poly(1-butene oxide). *Polymer* **1970**, *11*, 626−628.

(56) Rubinstein, M.; Colby, R. *Polymer Physics*. Oxford University Press; New York: 2003.

(57) Grulke, E. A.; Immergut, E.; Brandrup, J. *Polymer Handbook*. John Wiley & Sons, 1999.

(58) Hoy, K. L. New Values of the Solubility Parameters from Vapor Pressure Data. *J. Paint Technol.* **1970**, *42*, 76−118.

(59) Price, G. J.; Shillcock, I. M. Inverse Gas Chromatographic Measurement of Solubility Parameters in Liquid Crystalline Systems. *J. Chromatogr. A* **2002**, *964*, 199−204.

(60) Sorichetti, V.; Hugouvieux, V.; Kob, W. Structure and Dynamics of a Polymer-Nanoparticle Composite: Effect of Nano-

https://dx.doi.org/10.1021/acs.macromol.0c00158
Macromolecules XXXX, XXX, XXX−XXX

particle Size and Volume Fraction. *Macromolecules* **2018**, *51*, 5375−5391.

(61) Glomann, T.; Schneider, G. J.; Brás, A. R.; Pyckhout-Hintzen, W.; Wischnewski, A.; Zorn, R.; Allgaier, J.; Richter, D. Unified Description of the Viscoelastic and Dielectric Global Chain Motion in terms of the Tube Theory. *Macromolecules* **2011**, *44*, 7430−7437.

(62) Liu, C.; He, J.; van Ruymbeke, E.; Keunings, R.; Bailly, C. Evaluation of Different Methods for the Determination of the Plateau Modulus and the Entanglement Molecular Weight. *Polymer* **2006**, *47*, 4461−4479.

(63) Jouault, N.; Kumar, S. K.; Smalley, R. J.; Chi, C.; Moneta, R.; Wood, B.; Salerno, H.; Melnichenko, Y. B.; He, L.; Guise, W. E.; Hammouda, B.; Crawford, M. K. Do Very Small POSS Nanoparticles Perturb s-PMMA Chain Conformations? *Macromolecules* **2018**, *51*, 5278−5293.

(64) Rizk, M.; Krutyeva, M.; Lühmann, N.; Allgaier, J.; Radulescu, A.; Pyckhout-Hintzen, W.; Wischnewski, A.; Richter, D. A Small-angle Neutron Scattering Study of a Soft Model Nanofiller in an Athermal Melt. *Macromolecules* **2017**, *50*, 4733−4741.

(65) De Gennes, P. G. *Scaling Concepts in Polymer Physics*; Cornell University Press, 1979.

(66) Fox, T. G.; Flory, P. J. The Glass Temperature and Related Properties of Polystyrene. Influence of Molecular Weight. *J. Polym. Sci.* **1954**, *14*, 315−319.

(67) Ueberreiter, K.; Kanig, G. Self-plasticization of Polymers. *J. Colloid Sci.* **1952**, *7*, 569−583.

(68) Ferry, J. D. *Viscoelastic Properties of Polymers*; 4th ed.; John Wiley & Sons, 1980; Chapter 17, pp 486−515.

(69) Inoue, T.; Narihisa, Y.; Katashima, T.; Kawasaki, S.; Tada, T. A Rheo-Optical Study on Reinforcement Effect of Silica Particle Filled Rubber. *Macromolecules* **2017**, *50*, 8072−8082.

(70) Nusser, K.; Schneider, G. J.; Pyckhout-Hintzen, W.; Richter, D. Viscosity Decrease and Reinforcement in Polymer-Silsesquioxane Composites. *Macromolecules* **2011**, *44*, 7820−7830.

(71) Kalathi, J. T.; Grest, G. S.; Kumar, S. K. Universal Viscosity Behavior of Polymer Nanocomposites. *Phys. Rev. Lett.* **2012**, *109*, 198301.

(72) Chen, Q.; Gong, S. S.; Moll, J.; Zhao, D.; Kumar, S. K.; Colby, R. H. Mechanical Reinforcement of Polymer Nanocomposites from Percolation of a Nanoparticle Network. *ACS Macro Lett.* **2015**, *4*, 398−402.

(73) Payne, A. R. The Dynamic Properties of Carbon Back-loaded Natural Rubber Vulcanizates. Part I. *J. Appl. Polym. Sci.* **1962**, *6*, 57−63.

(74) Mullins, L. Softening of Rubber by Deformation. *Rub. Chem. Technol.* **1969**, *42*, 339−362.

(75) You, W.; Yu, W. Slow Linear Viscoelastic Relaxation of Polymer Nanocomposites: Contribution from Confined Diffusion of Nanoparticles. *Macromolecules* **2019**, *52*, 9094−9104.

(76) Chai, S. C.; Xu, T. Y.; Cao, X.; Wang, G.; Chen, Q.; Li, H. L. Ultrasmall Nanoparticles Diluted Chain Entanglement in Polymer Nanocomposites. *Chin. J. Polym. Sci.* **2019**, *37*, 797−805.

(77) Song, Y.; Zheng, Q. Concepts and Conflicts in Nanoparticles Reinforcement to Polymers beyond Hydrodynamics. *Prog. Mater. Sci.* **2016**, *84*, 1−58.

(78) Guo, B.; Tang, Z.; Zhang, L. Transport Performance in Novel Elastomer Nanocomposites: Mechanism, Design and Control. *Prog. Polym. Sci.* **2016**, *61*, 29−66.

(79) Einstein, A. A New Determination of Molecular Dimensions. *Ann. Phys.* **1906**, *19*, 289−306.

(80) Li, Y.; Kröger, M.; Liu, W. K. Nanoparticle Effect on the Dynamics of Polymer Chains and Their Entanglement Network. *Phys. Rev. Lett.* **2012**, *109*, 118001.

(81) Senses, E.; Ansar, S. M.; Kitchens, C. L.; Mao, Y.; Narayanan, S.; Natarajan, B.; Faraone, A. Small Particle Driven Chain Disentanglements in Polymer Nanocomposites. *Phys. Rev. Lett.* **2017**, *118*, 147801.

(82) Kalathi, J. T.; Kumar, S. K.; Rubinstein, M.; Grest, G. S. Rouse Mode Analysis of Chain Relaxation in Polymer Nanocomposites. *Soft Matter* **2015**, *11*, 4123−4132.

(83) Ganesan, V.; Pryamitsyn, V.; Surve, M.; Narayanan, B. Noncontinuum Effects in Nanoparticle Dynamics in Polymers. *J. Chem. Phys.* **2006**, *124*, 221102.

(84) Wang, M.; Hill, R. J. Anomalous Bulk Viscosity of Polymer-Nanocomposite Melts. *Soft Matter* **2009**, *5*, 3940−3953.

(85) Mackay, M. E.; Dao, T. T.; Tuteja, A.; Ho, D. L.; Van Horn, B.; Kim, H.-C.; Hawker, C. J. Nanoscale Effects Leading to Non-Einstein-like Decrease in Viscosity. *Nat. Mater.* **2003**, *2*, 762.

https://dx.doi.org/10.1021/acs.macromol.0c00158
Macromolecules XXXX, XXX, XXX−XXX